ful step toward discovering how this system serves so many aspects of learning. Such specific characterization has been limited largely to ablation studies in monkeys and rats. The present findings indicate that functional neuroimaging can provide insights about specialization of mnemonic processes in the human medial temporal-lobe memory system. Such specializations are likely both to parallel, owing to shared evolutionary histories, and to differ from, owing to what is uniquely human, those found in monkeys and rats.

REFERENCES AND NOTES

1. W. B. Scoville and B. Milner, *J. Neurol. Neurosurg. Psychiatry* **20**, 11 (1957); L. R. Squire, *Psychol. Rev.* **99**, 195 (1992).
2. R. Insausti, D. G. Amaral, W. M. Cowan, *J. Comp. Neurol.* **264**, 356 (1987).
3. L. E. Jarrard and T. L. Davidson, *Psychobiology* **18**, 68 (1990); H. Eichenbaum, T. Otto, N. J. Cohen, *Behav. Brain Sci.* **17**, 449 (1994); E. A. Murray, *Semin. Neurosci.* **8**, 13 (1996); D. Gaffan, *Exp. Brain Res.* **99**, 411 (1994); B. W. Leonard, D. G. Amaral, L. R. Squire, S. Zola-Morgan, *J. Neurosci.* **15**, 5637 (1995).
4. S. Ogawa, T. M. Lee, A. S. Nayak, P. Glynn, *Magn. Reson. Med.* **14**, 68 (1990); K. K. Kwong *et al.*, *Proc. Natl. Acad. Sci. U.S.A.* **89**, 5675 (1992); D. C. Noll, J. D. Cohen, C. H. Meyer, W. Schneider, *J. Magn. Reson. Imaging* **5**, 49 (1995).
5. Informed consent was obtained from all participants. Structural images were longitudinal relaxation time (T1)–weighted, flow-compensated spin-warp repetition time [(TR) = 500 ms, minimum echo time (TE)]. Eight functional images were collected every 2880 ms through use of a gradient echo spiral sequence sensitive to apparent transverse relaxation time (T2*) with four interleaves (TR = 720 ms, TE = 40 ms, flip angle = 65°). There were 984 (or 1808 in the control study) and 1296 (or 1520) functional images collected per subject for the retrieval and encoding tasks, respectively. Two 5-inch-diameter local receive coils were used with five subjects, and a whole head coil was used for the sixth subject and both subjects in the control study. Head movement was minimized through use of a "bite-bar" formed with each subject's dental impression; motion artifact was examined automatically for all scans.
6. Subjects viewed 80 line drawings presented twice 24 hours and once 30 min before scanning. During the 342-s retrieval scan, subjects saw eight sets of 20 words each presented individually for 1500 ms with 500-ms intervals between words. Alternate New and Old sets comprised, respectively, 18 new words (names of nonstudied drawings) and 2 old words (names of studied drawings) or 18 old words and 2 new words. Subjects were instructed visually to squeeze a pneumatic bulb for names of studied pictures in Old sets or for names of nonstudied pictures in New sets. During the 467-s encoding task, subjects saw 12 sets of eight pictures, with each set including four indoor and four outdoor scenes presented individually for 3000 ms with 1800-ms intervals between pictures. Alternate sets comprised New pictures not seen before and two Old pictures presented repeatedly. Subjects were instructed visually to squeeze for indoor scenes and to remember the pictures. The order of stimulus presentation (Old/New or New/Old) was counterbalanced across subjects for both tasks. The control study was identical in organization except that subjects studied 102 words three times each just before scanning; saw in the retrieval task (648 s) 12 sets of 17 line drawings each presented for 2000 ms with 1000-ms intervals in alternate blocks of 15 new and 2 old or 15 old and 2 new drawings; and responded to drawings of living objects in the encoding task (547 s) during which they saw 28 sets of four living and four nonliving objects each presented for 2000 ms with 500-ms intervals.
7. J. G. Snodgrass and M. Vanderwart, *J. Exp. Psychol. Hum. Learn. Mem.* **9**, 174 (1980).
8. C. E. Stern *et al.*, *Proc. Natl. Acad. Sci. U.S.A.* **93**, 8660 (1996).
9. Activation maps were determined by analyzing the correlation for each pixel between signal intensity and a reference function computed by convolving a square wave at the task frequency (alternating conditions in each task) with a data-derived estimate of the hemodynamic response function [K. J. Friston, P. Jezzard, R. Turner, *Hum. Brain Mapping* **1**, 153 (1994)]. Pixels were selected that (i) exceeded the statistical criterion of $z > 1.96$ (representing significance at $P < 0.025$, one-tailed) and (ii) were not eliminated with a 2 by 2 pixel median filter that eliminated isolated selected pixels.
10. For all subjects, the subiculum was outlined anatomically in three anterior sections and the parahippocampal cortex in three posterior sections without functional data overlays. Regions were defined by landmarks [D. G. Amaral and R. Insausti, in *The Human Nervous System*, G. Paxinos, Ed. (Academic Press, San Diego, CA, 1990), pp. 711–755; H. M. Duvernoy, *The Human Hippocampus* (Verlag, Munich, 1988)]. Percentages of significantly activated pixels were analyzed in a repeated-measures analysis of variance with factors of brain region (subiculum/parahippocampal cortex), hemisphere (left/right), and memory task (retrieval/encoding). The only significant effect was a region × task interaction, $F(1, 5) = 11.97$, $P = 0.018$, reflecting more activation in the subiculum during the retrieval than during the encoding task [$t(5) = 3.94$, $P = 0.01$], but more activation in the parahippocampal cortex during the encoding than during the retrieval task [$t(5) = 2.77$, $P < 0.05$]. There were also trends for more activation during the encoding than the retrieval task, and more activation in the parahippocampal cortex than in the subiculum (P values = 0.11).
11. L. R. Squire *et al.*, *Proc. Natl. Acad. Sci U.S.A.* **89**, 1837 (1992); D. L. Schacter, N. M. Alpert, C. R. Savage, S. L. Rauch, M. S. Albert, *ibid.* **93**, 321 (1996); D. L. Schacter *et al.*, *Nature* **376**, 587 (1995); L. Nyberg, A. R. McIntosh, S. Houle, L.-G. Nilsson, E. Tulving, *ibid.* **380**, 715 (1996); E. Tulving, H. J. Markowitsch, S. Kapur, R. Habib, S. Houle, *Neuroreport* **5**, 2525 (1994); C. L. Grady *et al.*, *Science* **269**, 218 (1995).
12. L. L. Jacoby, *J. Mem. Lang.* **30**, 513 (1991); G. Mandler, *Psychol. Rev.* **87**, 252 (1980); J. M. Gardiner, *Mem. Cognit.* **16**, 309 (1988).
13. W. A. Suzuki and D. G. Amaral, *J. Comp. Neurol.* **350**, 497 (1994).
14. S. Zola-Morgan. L. R. Squire, D. G. Amaral, W. A. Suzuki, *J. Neurosci.* **9**, 4355 (1989); M. Meunier, J. Bechevalier, M. Mishkin, E. A. Murray, *ibid.* **13**, 5418 (1993).
15. S. Zola-Morgan, L. R. Squire, D. G. Amaral, *ibid.* **6**, 2950 (1986); N. Rempel-Clower, S. Zola, L. R. Squire, D. G. Amaral, *ibid.* **16**, 5233 (1996).
16. B. T. Hyman, G. W. Van Hoesen, A. R. Damasio, C. L. Barnes, *Science* **225**, 1168 (1984); D. C. Davies, A. C. Wilmott, D. M. A. Mann, *Neurosci. Lett.* **94**, 228 (1988).
17. D. Gaffan and E. A. Gaffan, *Brain* **114**, 2611 (1991).
18. M. Bunsey and H. Eichenbaum, *Nature* **379**, 255 (1996).

19. Supported by grants from the National Institute on Aging and the National Center for Research Resources. J.B.B. was supported by a Medical Scientist Training Program grant awarded by the National Institute of General Medical Sciences. We thank two anonymous reviewers, C. Gabrieli, L. Marsh, L. Stefanacci, C. Stern, and S. Zola for advice on analyses and this manuscript.

22 October 1996; accepted 13 February 1997

Trafficking of Matrix Collagens Through Bone-Resorbing Osteoclasts

Stephen A. Nesbitt* and Michael A. Horton

An intracellular pathway for proteins liberated from mineralized matrix during resorption was identified in osteoclasts. Analysis by confocal microscopy of sites of active bone resorption showed that released matrix proteins, including degraded type I collagen, were endocytosed along the ruffled border within the resorption compartment and transcytosed through the osteoclast to the basolateral membrane. Intracellular trafficking of degraded collagen, as typified by the resorbing osteoclast, may provide the cell with a regulatory mechanism for the control of tissue degradation.

Osteoclasts are multinucleate bone cells with the capacity to degrade the extracellular matrix of the skeleton by the process of bone resorption, thus participating in the homeostasis of bone and calcium (*1*). Osteoclasts resorb mineralized tissues after a series of cellular polarization events (*2*). Cytoskeletal rearrangement creates an F-actin–rich structure, the tight seal, that encloses a specialized secretory membrane, the ruffled border. Protons and proteases cross the ruffled border and degrade bone matrix through demineralization and proteolytic activity, with calcium and type I collagen fragments being liberated into a resorption compartment beneath the cell. These products reach the extracellular space, where their levels correlate with bone resorption activity (*3*).

It has been assumed that degraded bone matrix leaves the resorption site by leakage from under the osteoclast during cell migration or is released en masse at the termination of the resorption cycle when the resorption compartment is disassembled. Alternatively, an enclosed resorption site could be maintained if there were intracel-

Bone and Mineral Centre, Department of Medicine, University College London Medical School, University College London, London WIN 8AA, UK.

*To whom correspondence should be addressed.

lular pathways to transport degraded bone through the osteoclast to the extracellular space, a process for which we provide three lines of evidence. Intracellular trafficking of mineralized matrix components was assessed in human osteoclasts [isolated from giant cell tumors of bone (*4*)] in a culture model of bone resorption that uses dentine substrate (*5*), and in osteoclasts resident in bone. Matrix proteins were localized at sites of resorption (*6*) by immunostaining and confocal microscopy (*7*, *8*).

Trafficking of matrix proteins through resorbing osteoclasts was identified with the use of a labeled dentine substrate (Fig. 1).

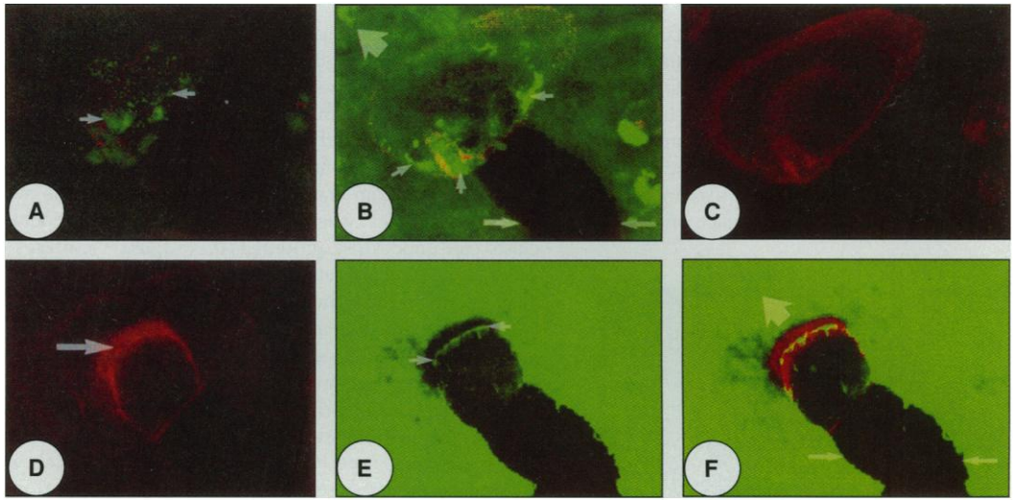

Fig. 1. (**A** to **F**) Trafficking of biotinylated dentine matrix proteins through resorbing osteoclasts. Human osteoclasts were cultured on biotinylated dentine slices for 24 hours (*6*, *7*). The cells were fixed and permeablized before fluorescent immunostaining and confocal microscopy (*8*). Sectional images (1-μm sections) from the *x-y* plane (above view) are shown for a typical resorbing osteoclast containing dentine matrix proteins (n = 51). The false colors of fluorescence represented are green (bone matrix proteins) and red (F-actin). Images are of sections taken at the following depths from the top of the osteoclast: (A) at 4 μm (shows the top of cell); (B) and (C) at 10 μm (showing the basolateral body of the cell); and (D), (E), and (F) at 20 μm (showing the cell at the dentine surface). The single fluorescent images show in (C), the spread cell periphery above the dentine surface; in (D), the ruffled border and location of the active resorption site that extended beneath the cell into the resorption pit (arrow, dense red F-actin arc structure); and in (E), a zone of liberated bone matrix proteins (small arrowheads) and loss of bone matrix to form the resorption pit (black). Double fluorescent images in (A) and (B) show the basolateral distributions of bone matrix proteins in the osteoclast (small arrowheads). Image (F) represents the images of (D) and (E) superimposed and reveals that the liberated matrix proteins are present within the ruffled border. The direction of osteoclastic resorption [broad arrowhead in images (B) and (F)] is indicated by the track of resorption left behind the osteoclast (pit edge shown by small arrows). The resorption pit extended 20 μm below the dentine surface through which the osteoclast maintained close contact with the resorbed surface of dentine [image (D), fine F-actin ring indicating the osteoclast periphery in the resorption pit]. Original magnification ×600.

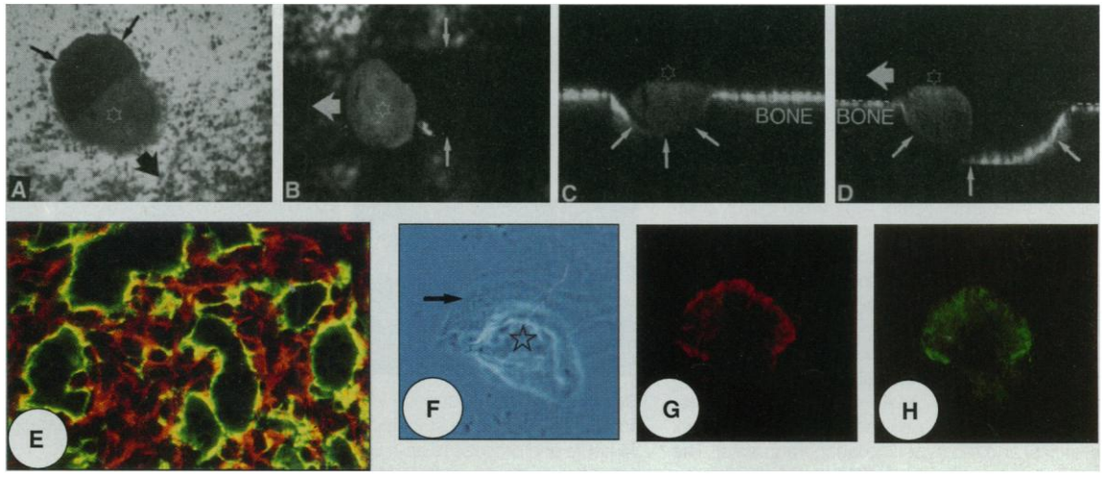

Fig. 2. (**A** to **D**) Trafficking of collagen in resorbing osteoclasts. Osteoclasts were cultured on dentine for 24 hours (*6*, *7*) and processed for immunostaining of collagen and confocal microscopy analysis (*8*). Sections (1 μm thick) of two of 116 osteoclasts assessed for type I collagen localization are shown. (A) shows an *x-y* section (above view) taken at the bone surface, (B) shows an *x-y* section taken 4 μm above the bone surface through the top of the osteoclast, and (C) and (D) show *z-x* sections (lateral views) for the cells in (A) and (B), respectively, taken through the center (broken lines denote the bone surface). The edge of the resorption pit is indicated by arrows; the tops of the resorbing osteoclasts are starred. Osteoclasts maintained close contact with the resorption face [arrows in (C) and (D)]. The direction of resorption (broad arrow) was indicated by the track left behind the osteoclast [pit edge is indicated by arrows in (A) to (D)]. Original magnification ×600. (**E**) Localization of collagen in osteoclasts within osteoclastoma tissue. Sections (10 μm thick) of osteoclastoma were immunostained and analyzed by confocal microscopy (*8*). Osteoclasts were identified by an antibody to the integrin $\alpha_v\beta_3$ which is highly expressed in osteoclasts (*22*). A 1-μm *x-y* section at 5-μm tissue depth is shown. False colors of fluorescence are green for $\alpha_v\beta_3$ on osteoclasts and red for type I collagen in the surrounding cells, and yellow reveals colocalization of collagen and $\alpha_v\beta_3$ at the osteoclast surface. Most osteoclasts are not in contact with bone and represent cells in a nonresorbing state. These had not endocytosed collagen, even though large amounts of collagen were visible in the surrounding tissue. Original magnification ×400. (**F** to **H**) Localization of collagen in osteoclasts in fetal bone. Collagen was identified in resorbing osteoclasts in frozen sections of human fetal bone. (F) is a nonconfocal phase image (osteoclast indicated by an arrow on bone trabeculum, open star). (G) and (H) are 1-μm *x-y* sections at 5-μm tissue depth for $\alpha_v\beta_3$ (red) and type I collagen fragments (green). Original magnification ×600.

Surface proteins in the dentine slices were biotinylated before osteoclast attachment and resorption and then detected with streptavidin-fluorescein (9). Resorption of matrix was seen as a loss of the surface biotin label and hence as an absence of specific staining (Fig. 1E). Many of the osteoclasts formed resorption tracks as they tunneled through the dentine and were identified at the end of the tracks by their characteristic F-actin staining pattern (Fig. 1, D and F). These ring- or arc-shaped structures are associated with the resorption compartment (2), and in tunneling osteoclasts, they indicate the position of the tight seal and ruffled border, which appose the surface undergoing resorption (Fig. 1F). Matrix components liberated into the resorption compartment (Fig. 1E) were detected within the ruffled border of the osteoclast (Fig. 1F). Many (92%; n = 51) of these osteoclasts had a distinct pattern of intracellular matrix proteins in which the proteins were localized within a cytoplasmic pool in the body (Fig. 1B) and toward the top of the osteoclast (Fig. 1A). These various staining patterns indicate that released matrix proteins were endocytosed along the ruffled border within the resorption pit and transcytosed through the osteoclast to the basolateral membrane facing the extracellular space, away from the resorbing surface.

Previous studies have suggested that osteoclasts can endocytose protein (*10, 11*). To investigate osteoclast endocytosis of matrix collagen, we probed the resorption cultures with an antibody to native type I collagen (Fig. 2, A to D). Intracellular localization of collagen in osteoclasts indicated that endocytosis of collagen from the extracellular dentine matrix was occurring because osteoclasts do not synthesize type I collagen (*12*). Confocal microscopy was used to generate images of 1-μm sections through the resorption cultures in both horizontal (x-y plane, above view in Fig. 2, A and B) and vertical planes (z-x plane, lateral view in Fig. 2, C and D). Type I collagen was located along the unresorbed bone surface and in the resorption pit. Collagen was seen only in the exposed regions of the pit where it had proceeded in a lateral direction and thus left a trail of resorption behind the osteoclast (Fig. 2D). Collagen was not detected throughout the dentine slice because it is impervious to antibody below a depth of 5 μm, a depth comparable with that achieved by biotinylation. Endocytosis of bone matrix collagens was identified in 97% of resorbing osteoclasts (n = 116). Generally, endocytosed collagen was localized throughout the cytoplasm of the osteoclast, with an additional focus toward the basolateral membrane, which faced the extracellular space (Fig. 2D). The pattern of intracellular collagen was comparable with that obtained for the biotinylated dentine matrix proteins (Fig. 1) and indicated that endocytosis and transcytosis of dentine matrix collagen was occurring through the osteoclast during resorption.

The trafficking of bone matrix proteins and collagens appeared to be initiated during the bone resorption process. These proteins were not detected in nonresorbing osteoclasts when examined in short-term cultures (*13*), nor in cultures where bone resorption was inhibited (*14*); nor were they detected in vivo in osteoclastoma tissue that had been separated from bone matrix and had no endogenous resorptive activity (Fig. 2E). However, intracellular collagen was detected in osteoclasts in contact with bone surfaces from human fetal tissue, which were exhibiting active trabecular resorption (Fig. 2, F to H) (*15*).

Bone collagens are extensively degraded by the action of collagenolytic enzymes during resorption (*16*). The resultant release of type I collagen fragments into the extracellular space and subsequent detection in plasma and urine provide a clinical measurement of bone resorption (*17*). The localization of collagen was assessed further in the human resorption cultures with antibodies that specifically recognize degraded collagen (*18*), and in resorbing rabbit osteoclasts (*13*). Degraded collagen was specific for the resorption site (Figs. 3 and 4). Osteoclastic resorption was assessed on biotinylated dentine substrates, which aided the

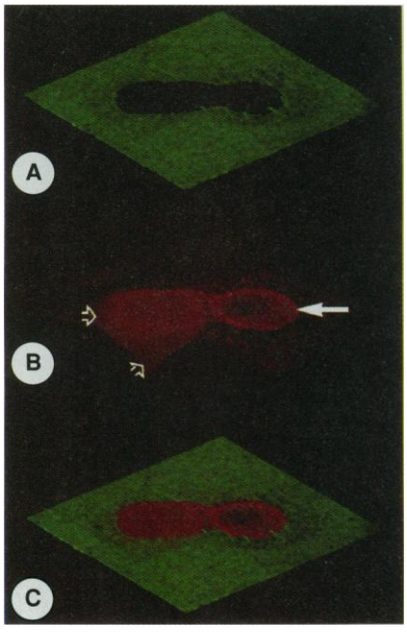

Fig. 3. (**A** to **C**) Trafficking of type I collagen fragments from dentine matrix through resorbing osteoclasts. Human osteoclasts were cultured on biotinylated dentine and processed as in Fig. 1 (*6–8*). Computer-generated compression images are shown for a typical resorbing osteoclast containing type I collagen fragments endocytosed from the dentine matrix (n = 105). Forty 1-μm x-y sections were taken through the resorption site and compressed into a single image and displayed on a 30% incline. False colors of fluorescence represented are green (biotinylated matrix proteins) and red (type I collagen fragments). The single fluorescent image in (A) shows the dentine matrix and resorption site (black), and the image in (B) indicates the localization of collagen fragments at the resorption site within two interconnected pits (the one on the right is indicated by an arrow). An osteoclast is located in the pit on the left (its spread cell periphery above the dentine surface is denoted by open arrows). Collagen fragments were observed in the pits and within the resorbing osteoclast. (C) is a superimposed image of (A) and (B) and shows that the type I collagen fragments are concentrated within the site of bone resorption. Original magnification ×600.

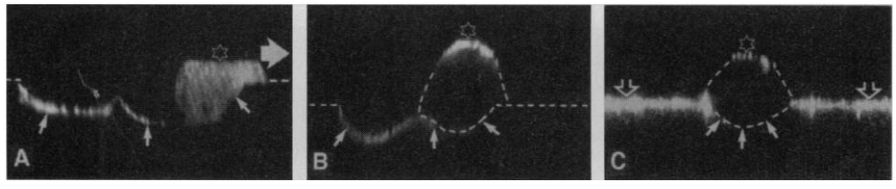

Fig. 4. (**A** to **C**) Cell surface localization of type I collagen fragments and biotinylated dentine matrix proteins in resorbing osteoclasts. Osteoclasts were cultured on unlabeled and biotinylated dentine for 24 hours and processed as in Fig. 1 (*6–8*). Lateral views are shown for 1-μm z-x sections taken through sites of resorption (n = 105). (A) and (B) show the localization of type I collagen fragments, (C) shows the localization of biotinylated matrix proteins, and (B) and (C) are nonpermeablized and show sites on the external surface of the osteoclast. Pits [arrows in (A) to (C)] extended below the dentine surface [indicated in (A) and (B) by horizontal broken lines; open arrows in (C) show the surface biotin label]. The tops of resorbing osteoclasts are starred. The cell membrane of osteoclasts are outlined in (B) and (C) by curved broken lines. Below the dentine surface osteoclasts are in close contact with the resorption site (curved broken line with arrows). Above the dentine surface, type I collagen fragments formed a basolateral "cap" at the cell surface in 80% of actively resorbing osteoclasts [image (B)]. Similar structures were seen with biotinylated bone matrix proteins in 15% of resorbing osteoclasts [image (C)]. Collagen fragments were absent from the unresorbed surfaces [horizontal broken lines in (A) and (B)]. Collagen fragments were also seen in resorbing osteoclasts with a focus in the basolateral aspect [image (A)]. The direction of osteoclastic resorption [broad arrow in (A)] was indicated by the track of resorption left behind the osteoclast. Original magnification ×600.

identification of the resorption sites through surface loss of the biotin label (Fig. 3A). An estimated 90% of type I collagen fragment immunostaining was within the resorption sites (Fig. 3, B and C, x-y tilted above view images, and Fig. 4A, z-x lateral view image). Intracellular localization in the osteoclast was comparable with that seen for type I collagen (Fig. 2). Degraded collagen lined the resorption pit. Additionally, collagen degradation was detected at a low level on the dentine surface surrounding the periphery of resorption pits, under the cytoplasmic skirt of the osteoclast (Fig. 3B). Thus, collagen degradation appears to be contained within the site of osteoclastic bone resorption and so provides evidence that the resorption compartment functions as an enclosed structure.

During bone resorption, the osteoclast maintains its ruffled border in close contact with the bone resorption surface (*19*), which suggests that, as the degraded bone matrix is liberated, it is continually cleared from these enclosed resorption sites. Thus, continual trafficking of the excavated bone matrix through the resorbing osteoclast to the extracellular space would seem essential if the cell is to maintain and contain bone resorption while resorbing further into the bone matrix. In support of this continual clearance of degraded matrix, biotin-labeled matrix proteins were not found in 81% of osteoclasts (n = 105) that were trafficking degraded collagens (Fig. 3C). These osteoclasts had resorbed through the 5-μm depth of the surface biotin label, thus suggesting that the initial endocytosed bone matrix proteins had been rapidly cleared through the osteoclast as resorption proceeded deeper into the dentine slice, typically 20 to 30 μm.

The intracellular localization of matrix proteins, type I collagen, and collagen fragments showed similar distribution patterns in resorbing osteoclasts, with a particular focus toward the basolateral region of the cell (Figs. 1, B and F, 2D, and 4A). Together, these results demonstrate that a general transcytotic pathway exists for degraded matrix proteins in resorbing osteoclasts, which appears to be analogous to the transcytosis of proteins across epithelial and endothelial cellular barriers (*20*). Transcytotic routes to the basolateral membrane have been implicated in bone-resorbing osteoclasts in studies with viral antigenic markers (*11*). These studies identified a central zone at the top of the basolateral membrane of the osteoclast that appeared to be a specialized site of exocytosis for resorbing osteoclasts, though this was not formally proven. Akin to this exocytotic site, type I collagen fragments and biotinylated matrix proteins were at the basolateral cell surface, forming a "cap" on a majority of resorbing osteoclasts (Fig. 4, B and C). The basolateral "cap" was absent from 15 to 20% of resorbing osteoclasts that had intracellular trafficking of degraded bone matrix proteins and collagens. This suggests that endocytosed and transcytosed degraded bone matrix collagens are released into the adjacent extracellular space from this region of resorbing osteoclasts.

The ruffled border in a resorbing osteoclast has been described as functionally equivalent to that of a secondary lysosome, being responsible for degradation of bone matrix within the confines of the resorption compartment (*21*). Intracellular trafficking of products resulting from tissue degradation may provide cells with a mechanism that enables them to monitor and hence control proteolytic activity; for the osteoclast this in turn would regulate the bone resorption process itself. Pharmacological intervention into this intracellular trafficking pathway for degraded extracellular matrix proteins may provide an approach to regulate tissue breakdown in disease.

REFERENCES AND NOTES

1. J. P. Bilezikian, L. G. Raisz, G. A. Rodan, Eds., *Principles of Bone Biology* (Academic Press, San Diego, CA, 1996).
2. H. K. Väänänen and M. Horton, *J. Cell Sci.* **108**, 2729 (1995).
3. N. T. Foged *et al.*, *J. Bone Miner. Res.* **11**, 226 (1996).
4. Giant cell tumors of bone (osteoclastomas) are rare bone tumors, but they provide a source of mature human osteoclasts that are otherwise impossible to extract from the hard matrix of bone. These cells are not the neoplasic cell type and have a normal phenotype and function [M. Horton *et al.*, *J. Pathol.* **144**, 282 (1984)].
5. T. J. Chambers and N. N. Ali, *J. Cell Sci.* **66**, 383 (1984); A. Boyde, N. N. Ali, S. J. Jones, *Br. Dent. J.* **156**, 216 (1984).
6. Resorption cultures of osteoclastoma osteoclasts were prepared as follows. Tissue was minced in ice-cold medium [minimal essential medium with Earles salts containing penicillin and streptomycin at 100 U/ml (MEM-PS) (Life Technologies, UK)]. Biotinylated and unlabeled dentine slices, which had been presoaked in culture medium (MEM-PS, 2% glutamine, and 10% fetal calf serum with 10 mM HCl to provide an operating pH of 6.9 at 5% CO_2) for 1 hour at 37°C in a humidified atmosphere of 5% CO_2, were seeded with the cell suspension for 2 hours. Nonadherent cells were rinsed off. The dentine slices, including an enriched population of osteoclasts, were cultured for 24 hours and fixed for 10 min in a 50:50 mixture of MEM with fixation buffer (3.5% paraformaldehyde and 2% sucrose in phosphate-buffered saline (PBS)].
7. Dentine preparation and labeling was done as follows. Blocks of elephant dentine were cut into slices (surface area 1 cm^2, thickness 100 μm), polished on 3MM paper, washed in water to remove debris, sterilized in 70% ethanol for 5 s, and dried. Slices were biotinylated by first washing them in 50 mM sodium bicarbonate buffer, pH 8.6, for 1 hour and then adding 500 μl of biotinylation buffer per dentine slice [490 μl of sodium bicarbonate buffer with 10 μl of biotinylation reagent, biotinamidocaproate *N*-hydroxysuccinamide ester (Amersham, UK)]. Biotinylation of matrix proteins proceeded for 1 hour at room temperature with mixing, followed by extensive washing in PBS for 3 hours.
8. Osteoclast immunocytochemistry and scanning laser confocal microscopy were done to assess the localization of type I collagen, F-actin, surface bone matrix proteins, and type I collagen fragments. Osteoclast numbers were accumulated from three experiments with separate tumors. Resorbing osteoclasts were identified by their characteristic F-actin structure by using phalloidin-rhodamine conjugate (5 U/ml, Molecular Probes, Netherlands) after 5 min of exposure at 4°C to permeablization buffer [20 mM Hepes, 300 mM sucrose, 50 mM NaCl, 3 mM $MgCl_2$, 0.5% Triton X-100 (Pierce and Warner, Chester, UK), and 0.5% sodium azide, in PBS at pH 7.0]. Biotinylated matrix proteins were probed with streptavidin-fluorescein (10 μg/ml, Vector Laboratories, UK). Rabbit polyclonal antibodies to native type I collagen were used at a 1/50 dilution (AB749, Chemicon, UK) with fluorescein isothiocyanate (FITC)–conjugated swine antibody to rabbit at a 1/40 dilution (Dakopatts, Denmark). Mouse monoclonal antibody (MAB A7), specific for degraded type I collagen, was provided by M. Bonde. Antibody MAB A7 was used at 10 μg/ml with FITC-conjugated goat antibody to mouse at a 1/20 dilution (Dakopatts, Denmark). Confocal microscopy was done as reported [P. Lakkakorpi, M. H. Helfrich, M. A. Horton, H. K. Väänänen, *J. Cell Sci.* **104**, 663 (1993)] using the Leica TCS NT and Bio-Rad MRC 600 or 1020 systems. No specific staining was seen if primary antibodies were omitted (*13*). Photomultiplier tube voltage thresholds for confocal microscopy were set to gate out background fluorescence given by immunoglobulin G (IgG)–negative controls. Fluorescent images were sequentially collected in 1-μm steps through osteoclasts for FITC and tetramethylrhodamine isothiocyanate fluorochromes at 488- and 568-nm emission wavelengths, respectively. The images were analyzed with Voxel View (Vital Images, Fairfield, IA) and Iris Indigo Graphics (Silicon Graphics, Mountain View, CA).
9. Biotinylation provided a suitable label for matrix proteins including type I collagen as assessed by SDS–polyacrylamide gel electrophoresis (PAGE). Biotinylation did not affect resorption; cell attachment and the number and area of resorption pits were comparable with resorption cultures on unlabeled dentine substrates (*13*).
10. M. E. Holtrop and G. J. King, *Clin. Orthop. Relat. Res.* **123**, 177 (1977).
11. J. Salo *et al.*, *J. Cell Sci.* **109**, 301 (1996).
12. M. Critchlow, Y. S. Bland, D. E. Ashurst, *Histochem. J.* **27**, 505 (1995); M. Critchlow, Y. S. Bland, D. E. Ashurst, *J. Cell Sci.* **107**, 499 (1994).
13. S. A. Nesbitt and M. A. Horton, unpublished data.
14. Inhibition of bone resorption with the cysteine proteinase inhibitor E64 (0.2 mM) (*3*) abolished the uptake of dentine matrix proteins (*13*).
15. Type I collagen was detected in 3% of osteoclasts in human fetal (14-week gestational age) bone sections. The lower frequency compared with osteoclast cultures reflects both the lower rate of resorption seen in vivo and the probability that many osteoclasts were not actively resorbing, even if on bone surfaces.
16. H. C. Blair *et al.*, *Biochem. J.* **290**, 873 (1993); F. Drake *et al.*, *J. Biol. Chem.* **271**, 12517 (1996).
17. R. Guerrero *et al.*, *Osteoporosis Int.* **6**, 297 (1996).
18. Antibody MAB-A7 was raised to an eight–amino acid sequence in the COOH-terminal telopeptide region of type I collagen, which is concealed in its native form and is exposed on degradation [M. Bonde, P. Quist, C. Fledelius, B. J. Riis, C. Christiansen, *Clin. Chem.* **40**, 2022 (1994)].
19. H. Zhou, R. Chernecky, J. E. Davies, *Cells Mater.* **3**, 141 (1993).
20. K. Simmons and S. Fuller, *Annu. Rev. Cell Biol.* **1**, 243 (1985); J. E. Rothman and F. T. Wieland, *Science* **272**, 227 (1996); K. E. Mostov *et al.*, *Cold Spring Harbor Symp. Quant. Biol.* **40**, 775 (1995).
21. R. Baron *et al.*, *J. Cell Biol.* **106**, 1863 (1988).
22. J. Davies *et al.*, *J. Cell Biol.* **190**, 1817 (1989).

23. This research was supported by the Imperial Cancer Research Fund and The Wellcome Trust. We thank T. Chaplin, A. Edwards, M. Helfrich, and P. Jordan for their kind assistance and the orthopedic surgeons at Royal Orthopaedic Hosptial, Birmingham, UK, for supplying tumor samples.

12 November 1996; accepted 7 February 1997